Final Report on

Microwave Power Transmission Using Electromagnetic Coupling of Open-Ring Resonators

Name of contractor	The University of Tokushima
Contract number	FA2386-11-1-40084
Report period	From June 28, 2011 to June 27, 2012
Author	Yasuo Ohno(Professor)
	Institute of Technology and Science, The University of Tokushima
	2-1 Minami-Josanjima, Tokushima 770-8506, Japan
	E-mail: ohno@ee.tokushima-u.ac.jp

Abstract

Experimental results on 60GHz band signal transmission through ECOR (Electromagnetic Coupling of Open-Ring Resonators) are shown. Through 200μm sapphire substrate, 60-70GHz band signal are transmitted with 58.9% transmission efficiency and 7.4GHz bandwidth. However, the transmission band was shifted about 10GHz higher frequency. The reason is under investigation.

ECOR technology is extended to lower frequencies for non-contact power transmission. The technology will benefit to power connectors for equipment modules where the problems caused by humidity and mechanical failure will be eliminated. A new diode structure for RF signal rectification, loss mechanism in rectenna circuits and the effect of wetting to ECOR transmission will be presented.

This report consists of the following four sections.

1. 60 GHz Wireless Interconnection Using ECOR
2. T-shaped Anode GaN Schottky Barrier Diode for Microwave Power Rectification
3. Analysis of Loss Mechanism in Rectenna Circuit
4. Effects of Wetting to Wireless Power Transmission by Open-Ring Resonators Coupling

Report Documentation Page

Form Approved
OMB No. 0704-0188

1. REPORT DATE	2. REPORT TYPE	3. DATES COVERED
01 NOV 2012	**Final**	**28-06-2011 to 27-06-2012**

4. TITLE AND SUBTITLE
Microwave Power Transmission Using Electromagnetic Coupling of Open-Ring Resonators

5a. CONTRACT NUMBER
FA23861114084

5b. GRANT NUMBER

5c. PROGRAM ELEMENT NUMBER

6. AUTHOR(S)
Yasuo Ohno

5d. PROJECT NUMBER

5e. TASK NUMBER

5f. WORK UNIT NUMBER

7. PERFORMING ORGANIZATION NAME(S) AND ADDRESS(ES)
The University of Tokushima,2-1 Minami-Josanjima-cho,Tokushima-shi 770-8506,Japan,JP,770-8506

8. PERFORMING ORGANIZATION REPORT NUMBER
N/A

9. SPONSORING/MONITORING AGENCY NAME(S) AND ADDRESS(ES)
AOARD, UNIT 45002, APO, AP, 96338-5002

10. SPONSOR/MONITOR'S ACRONYM(S)
AOARD

11. SPONSOR/MONITOR'S REPORT NUMBER(S)
AOARD-114084

12. DISTRIBUTION/AVAILABILITY STATEMENT
Approved for public release; distribution unlimited

13. SUPPLEMENTARY NOTES

14. ABSTRACT
Experimental results on 60GHz band signal transmission through ECOR (Electromagnetic Coupling of Open-Ring Resonators) are shown. Through 200μm sapphire substrate, 60-70GHz band signal are transmitted with 58.9% transmission efficiency and 7.4GHz bandwidth. However, the transmission band was shifted about 10GHz higher frequency. The reason is under investigation. ECOR technology is extended to lower frequencies for non-contact power transmission. The technology will benefit to power connectors for equipment modules where the problems caused by humidity and mechanical failure will be eliminated. A new diode structure for RF signal rectification, loss mechanism in rectenna circuits and the effect of wetting to ECOR transmission will be presented. This report consists of the following four sections: 60 GHz Wireless Interconnection Using ECOR, T-shaped Anode GaN Schottky Barrier Diode for Microwave Power Rectification, Analysis of Loss Mechanism in Rectenna Circuit, Effects of Wetting to Wireless Power Transmission by Open-Ring Resonators Coupling

15. SUBJECT TERMS
microwave devices and circuits, RF, Microwave Engineering

16. SECURITY CLASSIFICATION OF:			17. LIMITATION OF ABSTRACT	18. NUMBER OF PAGES	19a. NAME OF RESPONSIBLE PERSON
a. REPORT	b. ABSTRACT	c. THIS PAGE			
unclassified	**unclassified**	**unclassified**	**Same as Report (SAR)**	**22**	

1 60 GHz Wireless Interconnection Using ECOR[1]

1.1 ECOR

Several on-chip wireless interconnects have been proposed, such as antenna-type, capacitive coupling and inductive coupling. They are convenient to distribute signals on and out of chips, but the energy efficiency is too low to use the received signal without amplification. So, we proposed electromagnetic coupling of open-ring resonators (ECOR) to realize low-cost millimeter wave transceivers as shown in Fig.1.1 [2].

Resonator coupling is short distance but efficient transmission technology, so it has been used for meter-range wireless power transmission, such as WiTricity [3].

As device miniaturization has proceeded, CMOS can generate 60GHz signals, but the handling power is reduced. On the other hand, AlGaN/GaN HFETs can generate high power at millimeter wave range. To combine these technologies, conventional mechanical interconnection is not suited due to signal degradation and high assembly cost. So, we have ECOR to realize low-cost millimeter wave transceivers as shown in Fig.1.2 [4].

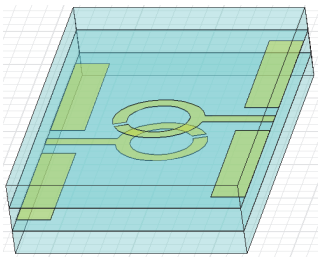

Fig.1.1. ECOR structure for HFSS simulation. All the substrates are assumed to be sapphire with isotropic dielectric constant of 10.

In the project last year we have designed ECOR for 60GHz signal transmission through sapphire wafers. We made gold wiring patterns of open-rings, CPW transmission lines and probe pads on sapphire and measured the transmission characteristics. 60 GHz range signals are transmitted through 200 μm thick sapphire substrate with 2.3dB insertion loss (58.9% transmission) and 7.4GHz bandwidth, but the transmission band are shifted about 10GHz higher frequencies.

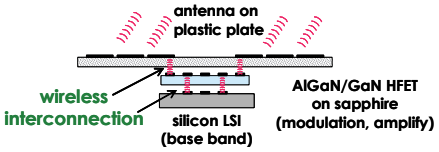

Fig.1.2. Schematic model of millimeter wave system using ECOR (Electromagnetic coupling of open-ring resonator).

1.2 Interconnect Structure

Open-ring resonator is a λ/2 resonator with circular shape to prevent radiation loss (Fig.1.3) [5]. When two resonators are placed closely, they couple electromagnetically and exchange energy wirelessly. Then, the resonant frequency splits and a band pass filter (BPF) is formed. The resonance occurs only within distance less than the wavelength. For 60GHz, it is

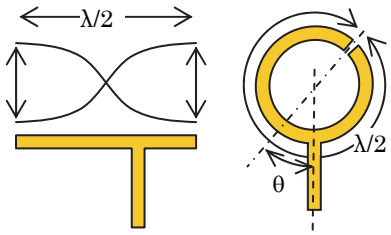

(a) (b)

Fig. 1.3. (a) simple λ/2 resonator which works as antenna, (b) open-ring resonator

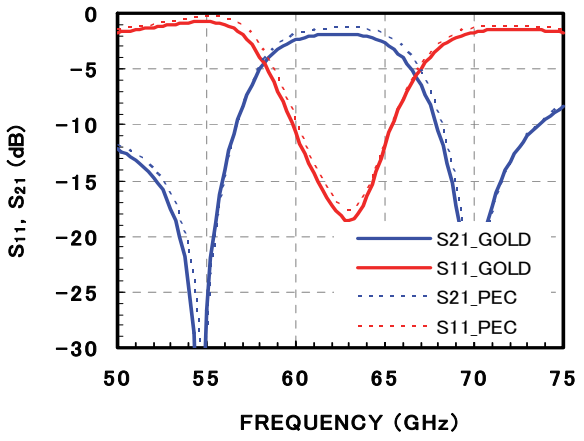

Fig.1.4 Simulated transmission characteristics through 200 μm sapphire substrate. θ=55°. S21 is transmission and S11 is reflection. PEC stands for perfect electric conductor.

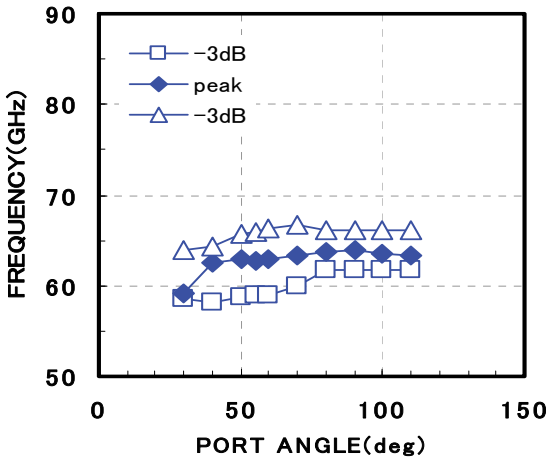

Fig.1.5 Simulated S21 peak frequency and the frequencies with -3dB (absolute value) as functions of port angle.

5mm in the air and 1.5mm in silicon or sapphire. Therefore, the ring diameter $d=\lambda/2\pi$, will be 230 μm on silicon or sapphire.

We performed electromagnetic simulation using HFSS (Figs.1.4-6). Through 200 μm thick sapphire substrate, 3dB band was formed from 58.1GHz to 66.4 GHz (bandwidth of 8.3GHz) with the minimum losses of 1.35 dB (73.3% transmission) for perfect electrical conductor (PEC) and 1.85 dB (65.3%) for gold wiring. Impedance matching to the signal feeder line is obtained by selecting the optimum port angle θ shown in Fig.1.3.

Fig.1.7 shows the peak transmission efficiency and 3dB bandwidth as function of the sapphire substrate thickness through which the signal travels. The transmission band is 5 GHz at the

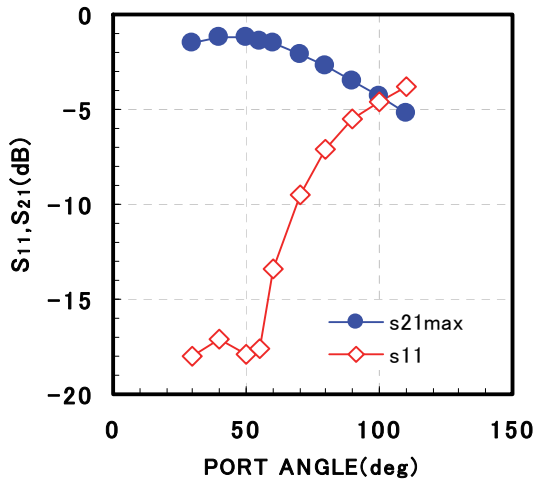

Fig.1.6 Simulated S21 peak value and S11 values at the same frequency, as functions of port angle.

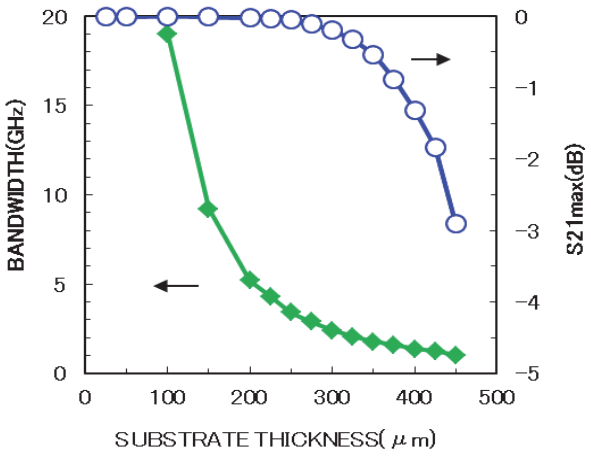

Fig.1.7 Simulated S21 peak value and the bandwidth as functions of sapphire substrate thickness.

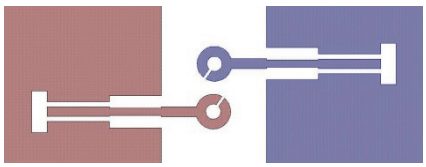

Fig.1.8 Open-ring resonator patterns for s-parameter measurement. Patterns for the two layers are shown. In the actual measurement, the rings are aligned to overlap. The ring outer diameter is 335μm.

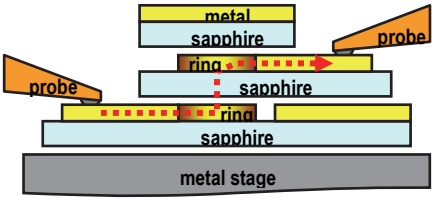

Fig.1.9 Schematic diagram of the measurement set up.

thickness of 200 μm and the band exists up to 400 μm.

1.3 Experiments

Based on the HFSS simulation, mask patterns are designed (Fig.1.8). The ring outer diameter is 335 μm and the inner diameter is 145 μm. 50Ω coplanar lines are connected to the rings for signal input and output.

The ring and lines are made on c-plane sapphire substrate with the thickness of 200 μm. Conventional photo lithography technology and electrolytic plating of gold are used to make the sample chips. The plated sample chips are overlapped, aligned and bonded with electron wax for the measurement. The measurement was carried out using Agilent E8361A and N5260A with the sample structure shown in Fig. 1.9.

The maximum transmission is obtained with the port angle of 80° and 55° as -2.3dB (58.9%) (Fig.1.10, 1.11, 1.12). From simulation, the losses are estimated as 0.5dB by conductor and 1.35 dB by radiation, maybe, by parallel plate mode propagating between the two metal planes. The obtained loss values are not so bad for the first experiment.

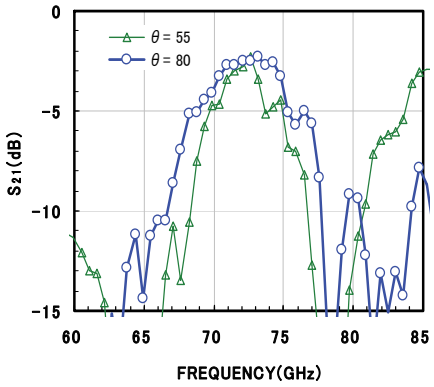

Fig.1.10 Measured S21 for the rings with port angles of 55° and 80°.

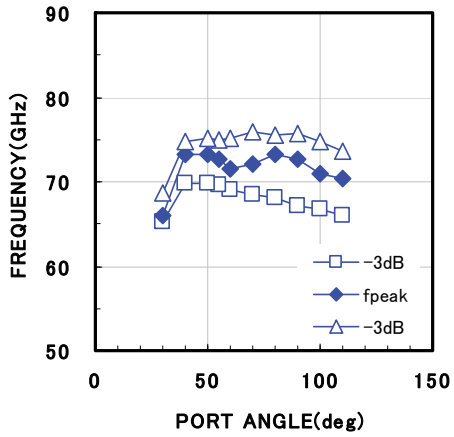

Fig.1.11 Measured S21 peak and the frequencies -3dB from the peak S21 value.

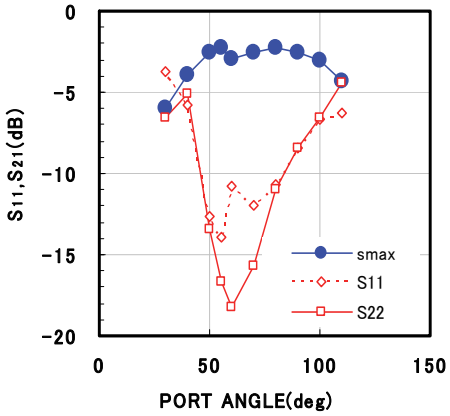

Fig.1.12 Measured S21 peak value and the S11 values at the same frequency.

For 80° port angle, bandwidth defined by -3dB frequencies from the maximum S21 is obtained as 7.4GHz (68.1~75.5GHz). The band is shifted about 10 GHz higher than simulated frequencies. The reason is not clear, but tuning will not be difficult for practical applications.

1.4 Conclusion

ECOR demonstrated 58.9% transmission efficiency and 7.4GHz bandwidth at 70GHz range for the wireless transmission through 200μm sapphire substrate.

ECOR has already been confirmed to works on high resistivity Si substrate (> 1 kΩcm) [6], and its alignment tolerance is so wide as around a half the ring diameter [7]. In addition, ECOR is easy to fabricate on any kind of material. It will contribute to low cost assembly and heterogeneous integration of millimeter wave devices.

2 T-shaped Anode GaN Schottky Barrier Diode for Microwave Power Rectification[8]

2.1 Introduction

Rectifying diode is a key device for rectenna circuit in microwave power transmission system. For high RF/DC conversion efficiency, the reduction of ON-resistance (R_{ON}) and OFF-capacitance (C_{OFF}) is essential. For power rectification, the voltage applicable to the diodes should be as high as possible. From these requirements, wide bandgap semiconductors are expected to be used due to their high breakdown field and high electron mobility. Breakdown field E_C of GaN is 330V/μm, which is about 10 times higher than that of silicon and GaAs. The electron drift mobility μ_0 at low doping level is about 1500cm^2/Vs, which is higher than that of silicon.

For actual diode design, several structure parameters should be considered, such as diode size and the doping concentrations . The anode structure of our previous device is shown in Fig.2.1 (a), where the breakdown voltage is assumed as 100V, so 10^{17}cm^{-3} donor concentration and 1μm active layer thickness were selected [9,10,11]. Field plate was used at the anode edge utilizing the alignment margin on Ni/Au layer for gold plating. The field plate showed the breakdown voltage increase from 93V to 108V, but also the depletion capacitance was increased about 25% in the zero voltage capacitance. In this chapter, we will show a diode with a new anode structure together with the improved epi-layer design so that the OFF capacitance and ON resistance will be reduced.

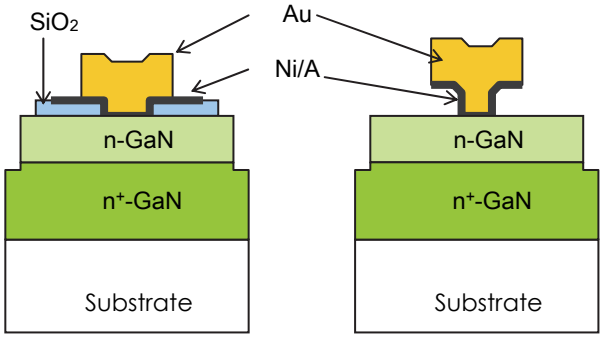

(a) (b)

Fig.2.1 Schematic cross section of GaN SBD. (a) Previous diode with field plate, (b) T-shaped anode diode.

2.2 GaN Schottky barrier diodes

Since there is no diffusion capacitance at injection condition, Schottky barrier diodes (SBD) are used for high frequency applications. From simple one-dimensional calculation, electrical characteristics of Schottky barrier diode is obtained. Assuming S for anode area, t for active layer thickness, N_D for donor concentration in the active layer and μ for electron drift mobility, the diode ON resistance is written as,

$$R_{ON} = \frac{t}{Sq\mu N_D}, \qquad (2.1)$$

where q is the unit charge. Also, the OFF

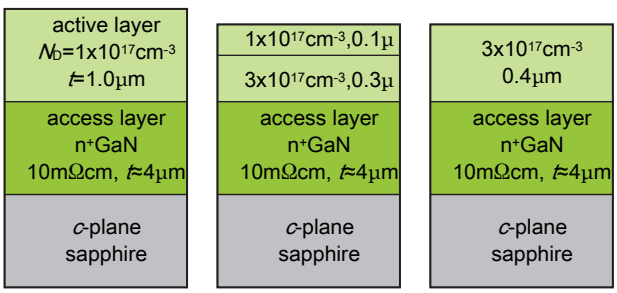

(A) (B) (C)

Fig.2.2 Epitaxial layer for the experiments. The sheet resistance of the access layer is about 25Ω.

capacitance under full depletion condition is given as,

$$C_{OFF} = \frac{\varepsilon_S S}{t}. \qquad (2.2)$$

Under these conditions, the bias voltage applied to the diode V_{MAX} is $qN_Dt^2/2\varepsilon_S$ where ε_S is the dielectric constant of the semiconductor. The field strength at the depletion edge is qN_Dt/ε_S and this value is E_C at the maximum voltage condition. Using these relations, the optimum epi-layer structure is given as,

$$t = \frac{2V_{MAX}}{E_C}, \qquad (2.3)$$

$$N_D = \frac{\varepsilon_S E_C^{\,2}}{2qV_{MAX}}. \qquad (2.4)$$

Using these relations, the time constant τ defined by the product of R_{ON} and C_{OFF} is given as,

$$\tau = R_{ON}C_{OFF} = \frac{2V_{MAX}}{\mu E_C^{\,2}}. \qquad (2.5)$$

Thus, wide bandgap semiconductors are suited for microwave rectifying application due to their high breakdown field.

2.3 T-shaped Anode Diode Structure

The device structure with T-shaped anode is shown in Fig. 2.1 (b). Fabrication process begins with the n-GaN layer etching to expose n^+-GaN layer by inductively coupled plasma (ICP) etching. Next, n^+-GaN layer is etched down to sapphire substrate for the isolation of bonding pads. Lift-off process is used for cathode Ohmic electrode with Ti/Al/Ni (50/200/50nm) and Ni/Au(10/40nm) successively. Annealing is carried out at 850°C for 1 minute in N_2 ambient.

Next, anode electrode opening is formed in photo-resist with the thickness of 2μm. Then, thin Ni/Au (10nm/10nm) layer is deposited over the whole wafer by sputtering. This layer will be used for electrode layer in

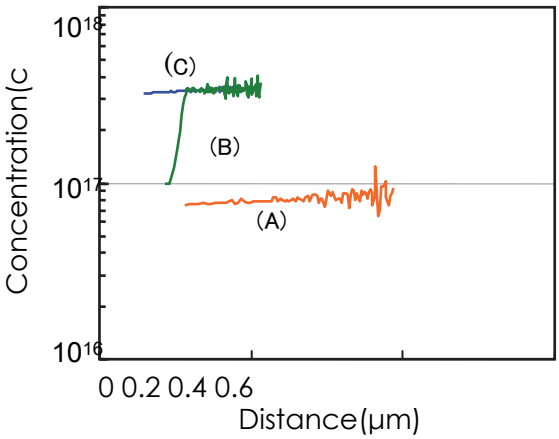

Fig.2.3 Impurity concentration obtained from 1MHz C-V measurement on 100μm diameter diodes.

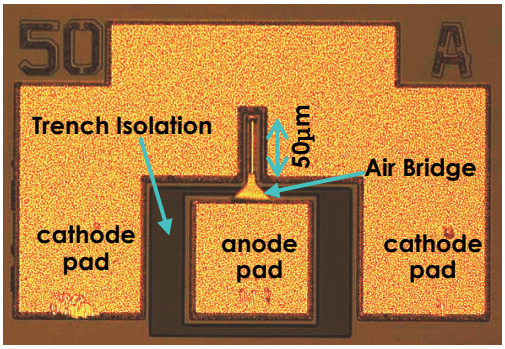

Fig.2.4 Photograph of one finger diode for s-parameter measurement.

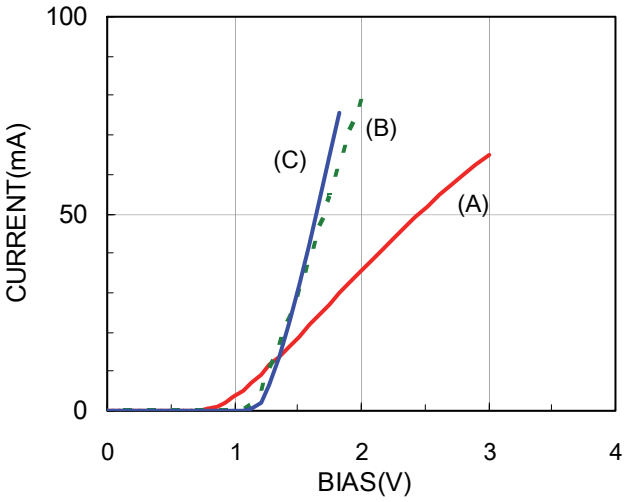

Fig.2.5 DC I-V characteristics.

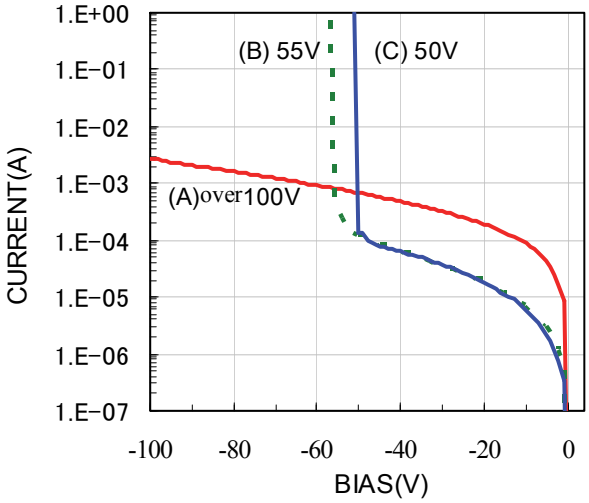

Fig.2.6 DC I-V characteristics in reverse direction.

gold electrolytic plating. The layer should be thin enough for the removal with the underlying photo-resist after the plating. Next, thick photo-resist pattern is formed for gold plating. The gold plating layer also forms air-bridge wiring between the anode electrodes and the bonding pads.

As discussed before, epi-layer design is important for low resistance and low capacitance. Since the peak to peak voltage of diode is about 4 times of the input signal amplitude, 100V peak to peak voltage corresponds to 25W input signal on 50 Ω line. The power value is large enough for the battery charging of small mobile equipment. So, we increased the donor concentration even with the decrease of breakdown voltage. Three epitaxial layers are prepared as shown in Fig.2.2. We call the diodes with the epi-structures as diodes (A), (B) and (C) in this paper. Fig. 2.3 shows the donor profile by 1 MHz C-V measurement on 100μm diameter circular diodes.

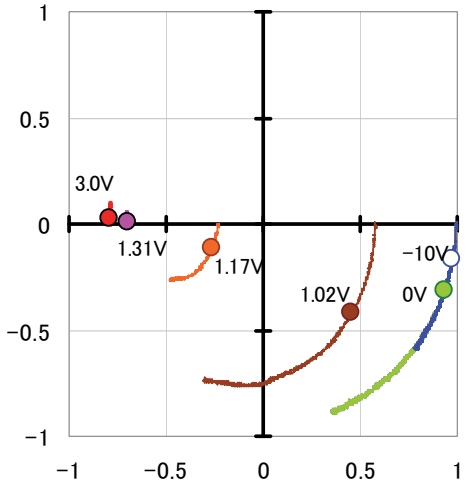

Fig. 2.7 S-parameters of diode (C) for different bias voltage. Frequency range is from 10MHz to 10 GHz and the dot indicate data at 2.45GHz.

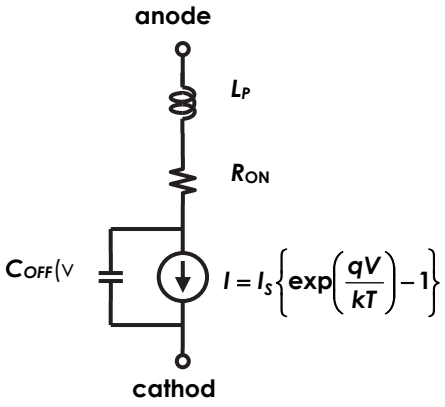

Fig. 2.8 Circuit model of the diodes estimated from s-parameter measurement.

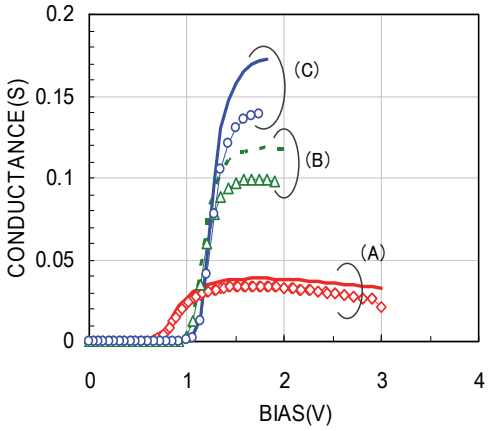

Fig.2.9 Conductance obtained from s-parameter measurement at 2.45GHz(lines) and that obtained from DC I-V characteristics shown in Fig. 5 (marks).

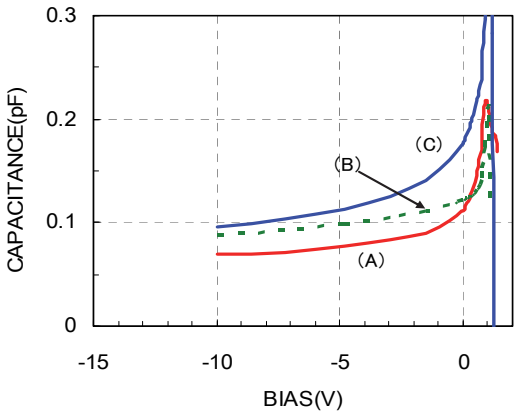

Fig.2.10 Capacitance obtained from s-parameter measurement at 2.45GHz.

Figure 2.4 shows the diode pattern for s-parameter measurement of one-finger diode. The finger size is 50μm long and 2μm wide. The pads for probing are separated by deep trench isolation down to sapphire substrate.

Table 2.1 Summary of the diode characteristics.

Device	Ref[7] *	(A)	(B)	(C)
N_D (cm^{-3})	$1x10^{17}$	$1x10^{17}$	$1x10^{17}$ +$3x10^{17}$	$3x10^{17}$
R_{ON} (Ω)	16.4	26.3	8.47	5.78
C_{j0} (pF)	0.180	0.112	0.122	0.178
C_{ave}** (pF)	0.166	0.137	0.107	0.090
$R_{ON}C_{ave}$ (ps)	1.90	3.55	0.91	0.52
V_F (V)	0.8	0.86	1.12	1.16
V_B (V)	108	100+	55	50

* converted into 2μm x 50μm size finger.
** average from 0 to -10V.

2.4 Electrical Performance

Figure 2.5 shows DC I-V characteristics of one-finger diodes. Turn on voltage defined at 1mA is 0.86V for diode (A) while it is around 1.15V for diodes (B) and (C), respectively. The reason of the difference is not clear. Surface condition may be different. Figure 2.6 shows I-V characteristics in reverse direction. The breakdown voltage is 55V for diode (B) and 50V for diode (C). Due to our equipment limitation, diode (A) did not show breakdown up to 100V.

S-parameters were measured using Agilent E8364B network analyzer with a source monitor unit Agilent E5263A. Measurement is carried out from 10MHz to 10GHz changing bias voltage. Measured data on diode (C) are shown in Fig. 2.7. Trajectories similar to typical RC series connection are appeared in reverse bias conditions including zero bias. As the forward bias voltage increases, conductance parallel to the capacitance appears and finally it shrinks to a pure low resistor circuit. For high forward bias condition, a small inductance around 50pH was appeared. From these, we estimate the diode can be modeled by the components as shown in Fig. 2.8.

Figure 2.9 shows conductance obtained from s-parameters at 2.45GHz. Conductance calculated from DC I-V characteristics is also shown. The difference between 2.45GHz and DC may come from the lack of cable resistance calibration in DC measurement.

Figure 2.10 shows the capacitance obtained from s-parameters at 2.45GHz. Capacitance increases as the reverse bias voltage decreases, but it sharply decrease at the onset of forward current. This is the typical characteristics of Schottky barrier diodes.

Diode characteristics are summarized in Table 2.1. Time constants are calculated using the average capacitance from zero to -10V, which may be suitable for the evaluation of actual circuit performance. Time constant τ is reduced is reduced from 1.90ps of the previous device to 0.52ps of device (C), while the breakdown voltage decreased from 108V to 50V.

Though similar epi-structure is used, τ is much larger for the present (A) structure than the previous device. Crystal quality might be better for the previous one, since the substrate for the epitaxial growth was SiC, which lattice constant is more closely matched to GaN than that of sapphire. Device (B) has low capacitance at zero voltage but the average capacitance is not so low and ON resistance is relatively high. Non-uniform doping may not be good to realize low ON resistance and low OFF capacitance simultaneously.

2.5 Conclusion

With T-shaped anode structure together with increased donor concentration for the active region, both ON resistance and OFF capacitance can be decreased. The time constant defined by the product of R_{ON} and C_{ave} decreased from 1.9ps to 0.52ps, but the breakdown voltage decreased from 108V to 50V.

For non-contact battery charging to mobile equipment, the efficiency will be improved with this diode. Step type doping profile did not show any particular merit indicating that uniform doping may be the optimum. However, the doping level should be determined depending on the maximum application voltage.

3 Analysis of Loss Mechanism in Rectenna Circuit[12]

3.1 Introduction

Microwave power transmission system requires high efficiency rectenna circuits for RF to DC conversion [9,13]. Two factors determine the conversion efficiency, reflection at the input port and the loss in diode.

Reflection is caused by the impedance mismatch between the input line and the rectenna circuit. Since the impedance of diodes varies with input bias and higher harmonics are generated in the rectification, the matching is a difficult task. It will, however, be achieved to a certain level by designing the input filter. We will not consider this matter in this paper, and will concentrate on the diode rectification efficiency in this report.

Diode rectification efficiency is determined by the ratio of DC output power against the input power to the diode, which is the signal source power subtracted by the reflected power. We will call this efficiency as "diode efficiency" and express as η_{DIODE}. To improve the diode efficiency, the reduction of the time constant τ defined by the product of ON resistance (R_{ON}) and OFF capacitance (C_{OFF}) is necessary. From one-dimensional analysis, τ can be obtained as [10],

$$\tau = R_{ON} C_{OFF} = \frac{2V_{MAX}}{\mu E_C^{\,2}}, \qquad (3.1)$$

where V_{MAX} is the maximum applicable voltage for the diode, μ is the electron drift mobility and E_{C} is the breakdown field strength. Due to high breakdown field and high electron mobility, GaN is expected as a high performance Schottky barrier diode (SBD). In actual circuit design, however, the capacitance and the resistance should be optimized separately even if their product τ is the same values.

In this paper, we will investigate the optimum combination of the capacitance and resistance under given

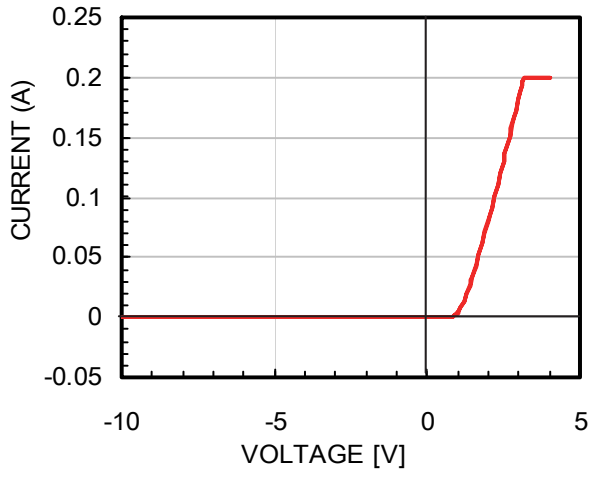

Fig. 3.1 *I-V* characteristics of one finger diode

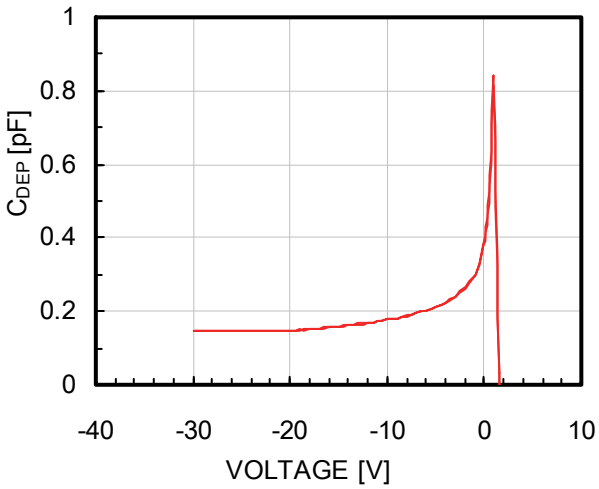

Fig. 3.2 *C-V* characteristics of one finger diode

operation conditions using circuit simulator. Comparing the simulation results, analytical expressions are developed which can estimate rectenna performance from the device and circuit parameters, such as input power, output load resistance and the signal frequency.

3.2 Rectenna Circuit Simulation with GaN SBD

Figure 3.1 shows I-V characteristics of one finger GaN Schottky barrier diode on SiC substrate [11]. The finger size is 2 μm x 100 μm. The ON resistance R_{ON} is 8Ω and V_F is 1.0V. Figure 3.2 shows the capacitance of the one-finger diode obtained from s-parameter measurement at 2.45GHz. The diode showed the breakdown voltage around 80V. On the same wafer, 5, 10 and 15 finger diodes are prepared for actual circuit use.

For optimum design of rectenna circuits using the diodes, we performed circuit simulation with Microwave Office. In the simulation, we used the pn-diode model of SPICE as shown in Fig. 3.3. The parameters are determined from the one finger diode measurement. To fit the *C-V* curve, a constant capacitance C_P is introduced as shown in the figure. R_{ON} is placed out of the diode.

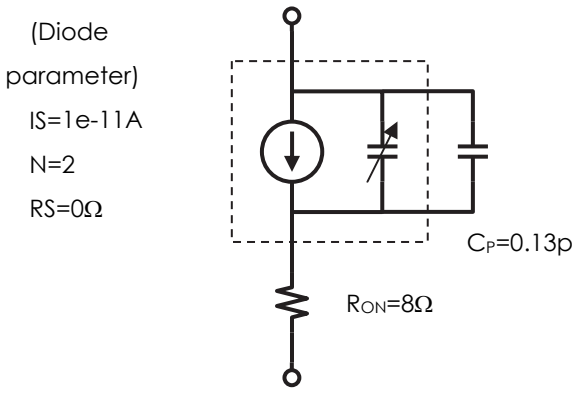

Fig. 3.3 Diode model used in circuit simulation. CP and RON placed out of the intrinsic diode model.

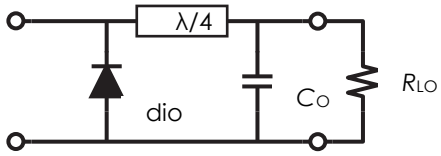

Fig. 3.4 Rectenna circuit used in the circuit

Figure 3.4 shows the typical rectenna circuit using λ/4 line. RF power is supplied from the signal source. Part of the power is converted into DC power and dissipated in the load resistor. The other part is dissipated in the diode as a power loss. The remaining part is reflected to the signal source including the higher harmonics generated during rectification.

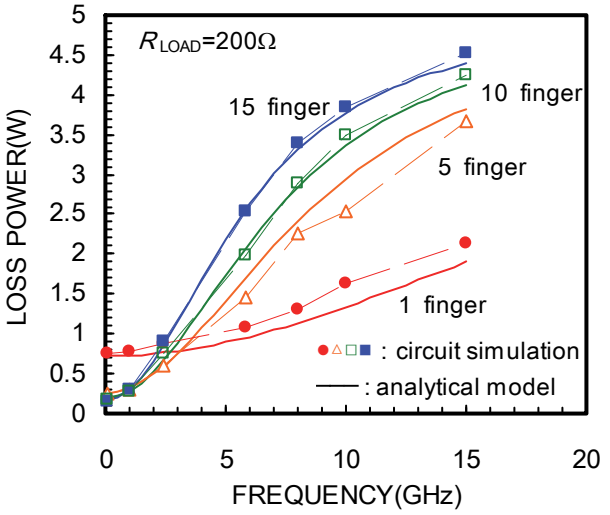

Fig. 3.5 Simulated loss power in diode as function of signal frequency in case of R_{LOAD}=200Ω. Values obtained by analytical model are obtained.

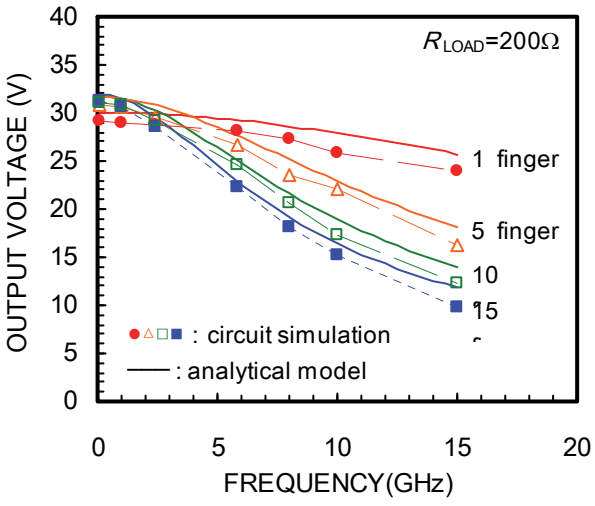

Fig. 3.6 Simulated output DC voltage as function of signal frequency in case of R_{LOAD}=200Ω. Values obtained by analytical model are obtained.

We put the signal source power as P_{IN}, the reflected power as P_{REF}, the diode loss power as P_{LOSS} and the DC output power as P_{DC}. Then, the diode efficiency η_{DIODE} is given as,

$$\eta_{DIODE} = \frac{P_{DC}}{P_{IN} - P_{REF}}. \qquad (3.2)$$

Since we would like to investigate the diode efficiency, P_{IN}-P_{REF} is kept constant in the simulation by tuning P_{IN} value.

Figure 3.5 shows the diode loss power P_{LOSS} as functions of signal frequency for diodes with different finger numbers. The load resistance R_{LOAD} is 200Ω. At low frequencies, the loss reduces as the finger number increases. This is due the reduction of ON resistance. As the signal frequency increases, the loss increases. The variation is larger for diodes with high finger number. This may be due to the loss by the increased capacitance during OFF state.

Figure 3.6 shows the output DC voltage. Since the load resistance is constant, the output voltage decreases as the diode loss power increases. Figures 3.7 and 3.8 are results in the case of R_{LOAD}= 40Ω. Due to the lower resistance, the output DC voltage is lower, but similar dependencies on the finger number and the frequency are obtained.

3.3 Analytical Model

To investigate the loss mechanism in rectenna circuits, analytical expression of the loss power is developed. In this analysis, diode characteristics are simplified as shown Fig. 3.9. Forward *I-V* curve is expressed only by R_{ON} and V_F values. Depletion capacitance $C_{DEP}(V)$ is replaced by a constant capacitance C_{OFF}.

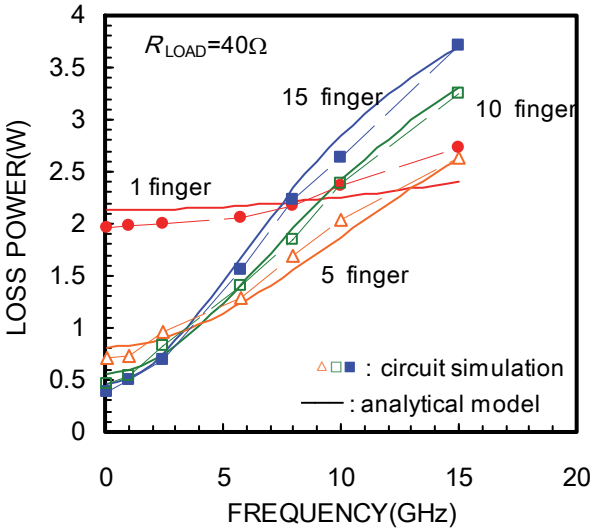

Fig. 3.7 Simulated loss power in diode as function of signal frequency in case of R_{LOAD}=40Ω. Values obtained by analytical model are obtained.

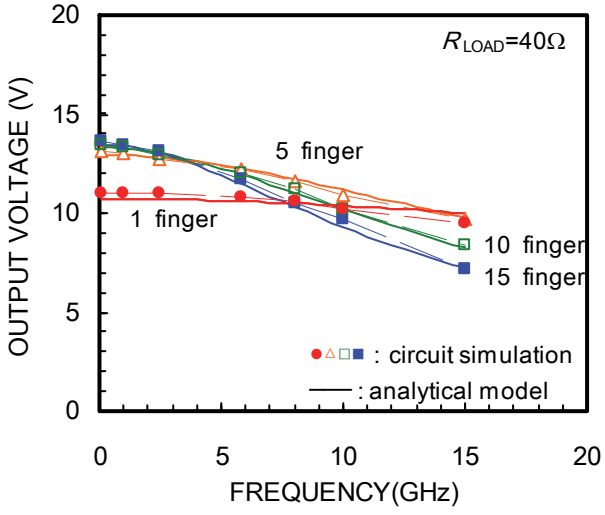

Fig. 3.8 Simulated output DC voltage as function of signal frequency in case of R_{LOAD}=40Ω. Values obtained by analytical model are obtained.

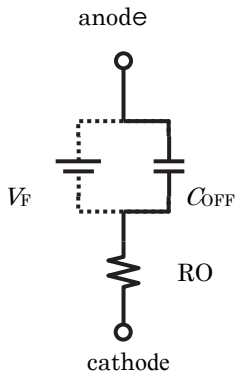

Fig. 3.9 Diode model used for analytical analysis. Dotted line indicates ON state path where current flows against the fixed voltage of V_F.

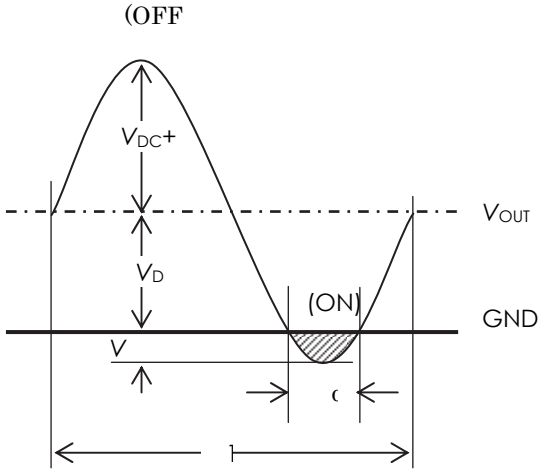

Fig. 3.10 Assumed wave form applied on the diode. Though the signal is sinusoidal, current in ON states is assumed constant.

When the DC output voltage value is V_{DC}, DC output power P_{DC} is given as,

$$P_{DC} = \frac{V_{DC}^{\ 2}}{R_{LOAD}}. \qquad (3.3)$$

The power dissipated in the diode can be divided into two parts, (a) ON state and (b) OFF state. In ON state, forward DC current flows. The average of the current should be the same as that of output DC current in a whole cycle, but it flows a certain short period as shown in Fig. 3.10. We put the ratio of the period as α. This value is less than 0.5 and we assumed 0.3. Then, the power consumed by the ON current is given as,

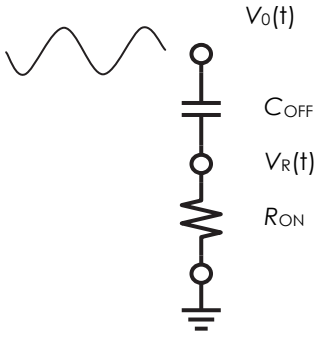

Fig. 3.11 Model for OFF state loss calculation. Sinusoidal wave which amplitude is V_{DC}+V_F is applied on the series connection of C_{OFF} and R_{ON}.

$$P_{LOSS\_ON} = \alpha\left\{V_F\left(\frac{V_{DC}}{\alpha R_{LOAD}}\right) + R_{ON}\left(\frac{V_{DC}}{\alpha R_{LOAD}}\right)^2\right\} \qquad (3.4)$$

The first term in the parentheses is by the voltage drop of the diode and the second term is by the diode resistance R_{ON}. The parameter α before the parentheses indicates the ratio of the state to the whole period.

The loss in OFF state is the displacement current by the depletion capacitance. Then, R_{ON} dissipates heat. We estimate the loss by a simplified model shown in Fig. 3.11, where a sinusoidal signal with the amplitude of V_F + V_{DC} is applied to the series connection of a capacitor and a resistor. The current flowing the resistor can be obtained by simple AC analysis as,

$$I = \frac{2\pi f C_{OFF}\left(V_F + V_{DC}\right)\left(i + 2\pi f C_{OFF} R_{ON}\right)}{1 + \left(2\pi f\right)^2 C_{OFF}^{\ 2} R_{ON}^{\ 2}} e^{i2\pi ft}, \qquad (3.5)$$

where f is the signal frequency. At low frequencies where $2\pi f C_{OFF} R_{ON} << 1$, the loss by the resistor is,

$$\begin{aligned} P_{LOSS\_OFF} &= R_{ON}|I|^2 \\ &= 4\pi^2\left(C_{OFF}^{\ 2} R_{ON}\right) f^2 (V_{DC} + V_F)^2 . \end{aligned} \qquad (3.6)$$

Then, input power to the diode P_{DIODE} can be written as,

$$\begin{aligned} P_{DIODE} &= P_{IN} - P_{REF} \\ &= P_{DC} + P_{LOSS\_ON} + P_{LOSS\_OFF} \quad . \end{aligned} \tag{3.7}$$

Assuming α value, VDC can be obtained solving Eq.(3.7) with Eqs. (3.3),(3.4) and (3.6). Then, all the powers including the loss power can be obtained. For multi-finger diodes, R_0 and C_0 $R_{\mathrm{ON}}=R_0/n$ and $C_{\mathrm{OFF}}=nC_0$, where R_0 and C_0 are the ON resistance and OFF capacitance of one finger diode, respectively, and n is the finger number.

The calculated lines are shown in Figs. 3.5 and 3.7 for the loss power and Figs.3.6 and 3.8 for V_{DC} together with the numerical simulation results. Here, V_{F}=0.8V, R_0=8Ω and α=0.3 are assumed. Good matching is obtained assuming C_0=0.17pF for R_{LOAD}=200Ω and C_0=0.24pF for R_{LOAD}=40Ω. They showed good agreements with the simulation results on both frequency dependency and the finger number dependency. The difference of the fitted capacitance values comes from their reverse bias voltage range. For R_{LOAD}=200Ω, DC voltage is 35V meaning the maximum voltage is about 70V, where as R_{LOAD}=40Ω, the maximum voltage is about 36V.

3.4 CONCLUSION

Loss mechanism of rectenna circuits are analyzed using a circuit simulator and an analytical model is developed. From the model, it is clarified that the low R_{ON} is important at low frequencies, but C_{OFF} is serious at high frequencies due to the parabolic dependency of the loss power on C_{OFF} and frequency. To improve the rectenna efficiency, the optimization of R_{ON} and C_{OFF} is important along with the reduction of their product.

We used a simple diode model in this analysis, but actual diodes have several parasitic capacitances and resistances depending on their structures. So, the more detailed modeling of Schottky barrier diodes based on actual measurements will be needed for more accurate estimation.

4 Effects of Wetting to Wireless Power Transmission by Open-Ring Resonators Coupling[14]

4.1 Introduction

A variety of mobile devices, such as mobile phones, digital cameras, and portable music players, could benefit from the use of wireless power transmission for battery charging. Since the data can be exchanged wirelessly, the only remaining external electric terminal for these devices is the power supply.

Electromagnetic coupling of open-ring resonators (ECOR) is an efficient non-contact power transmission technology [2] which can transmit microwave power through plastic plates. Combining an efficient rectenna circuit with a GaN Schottky barrier diodes (SBD), this technology offers a convenient power transmission system for battery charging of these devices.

Mobile equipment is often used in wet environments, so waterproof properties are highly desirable. Present waterproof equipment requires keeping electrical terminals dry during charging to prevent electric shock, charge leakage, and the corrosion of the metal electrodes. In addition, present devices require shielding the terminal by closing the cover carefully, which may be made difficult due to mechanical or material degradation.

A more convenient charging system would allow charging to be done in wet environments or even in water without any special measures or operations. Since the dielectric constant of water is as high as 80 and water exhibits dielectric losses, power transmission characteristics will be influenced by water. We have investigated the effect of wet conditions on an ECOR system operating at 2.45GHz.

4.2 Open-ring resonator Structure

ECOR is being developed for wireless signal interconnection between high-speed integrated circuits [2]. The rings are λ/2 resonators with the diameter of λ/2π. Impedance matching is obtained by selecting the connecting point with the signal feeder line on the ring circle. We previously applied ECOR technology for power transmission at 2.45 GHz targeting the application of mobile equipment battery charging [9]. In the experiments, the circuits were formed on a FR-4 glass epoxy printed board (ε = 4.7, t = 1.6mm, tan δ = 0.02) as shown in Fig. 4.1. The ECOR by itself showed 70.1 % transmission efficiency through the 1.6mm FR-4 board in the small signal measurement. Combining the ECOR with a GaN SBD, RF/DC conversion efficiency of 37.1 % was

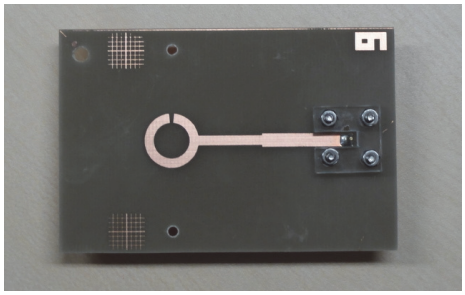

Fig.4.1. Photograph of printed board with an open-ring pattern.

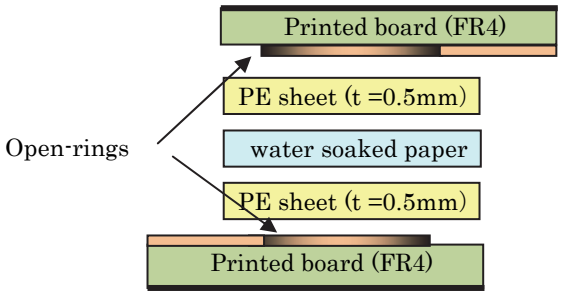

Fig.4.2. Sample structure for wet condition effect measurement

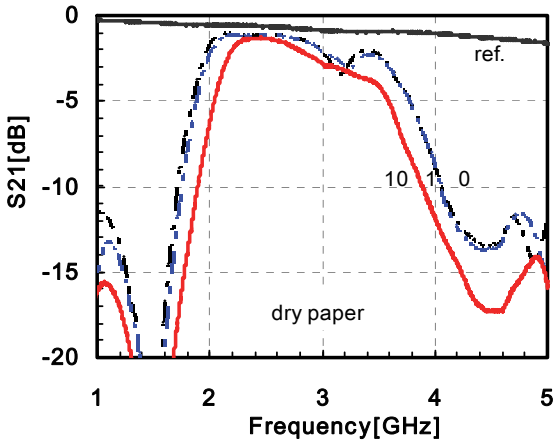

Fig.4.3. Transmission through dry paper. The numbers indicate the number of inserted paper sheets. The "ref" line indicates the transmission using a micro-strip line with the same distance between the connectors.

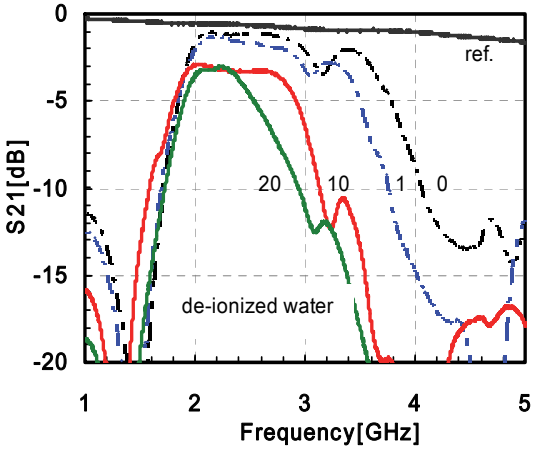

Fig.4.4. Transmission through de-ionized water. "0" indicates the case of no sheets of paper under dry conditions.

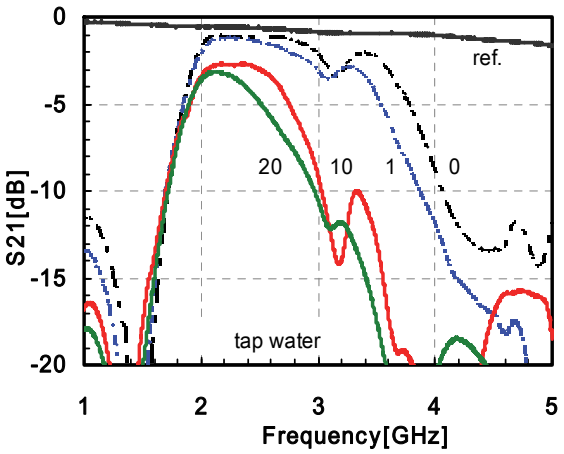

Fig.4.5. Transmission through tap water.

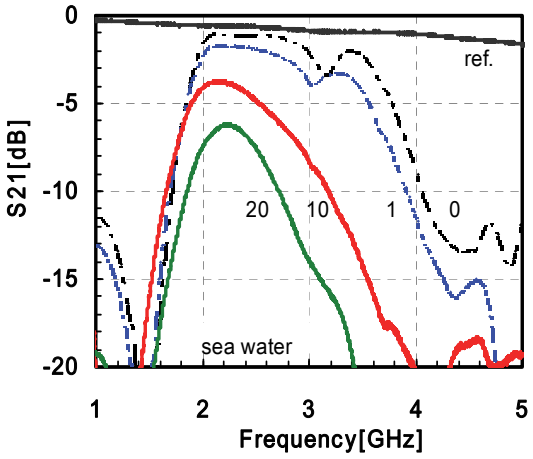

Fig.4.6. Transmission through sea water.

obtained at an input power of 3.01 W and frequency of 2.3 GHz.

The device structure for the present experiment is designed for 2.45GHz signal transmission. The ring diameter is 9.9mm. The signal is fed through a 50Ω micro-strip line. The rings are connected to an SMA connector through the micro-strip line with 18 μm thick copper. The back side of the board is covered with copper which is used as a ground plane. To achieve the best matching for the transmission through 1 mm thick polyethylene (PE) plate, the insertion angle to the ring is set 100° from the center of the ring circumference.

4.3 Experiment

In the measurement, two 0.5 mm thick PE boards were inserted between the printed boards (Fig.4.2). Sheets of clean-wipe paper, immersed in de-ionized water, tap water, or seawater, were inserted between the PE boards. The de-ionized water was obtained from our clean room, and the seawater was taken from the sea near Naruto strait.

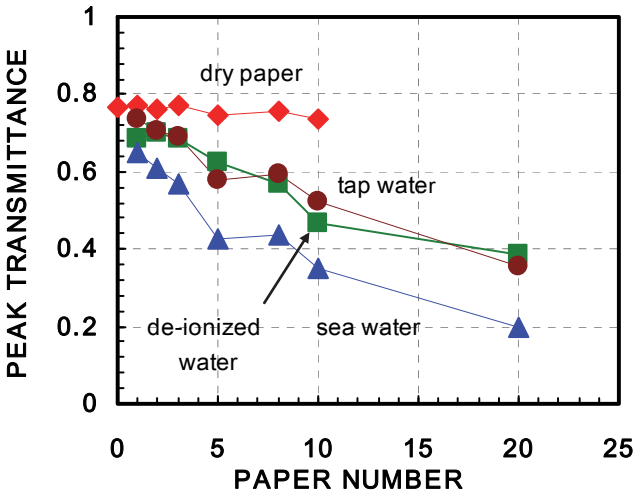

Fig.4.7. Peak transmittance as a function of the number of inserted paper sheets.

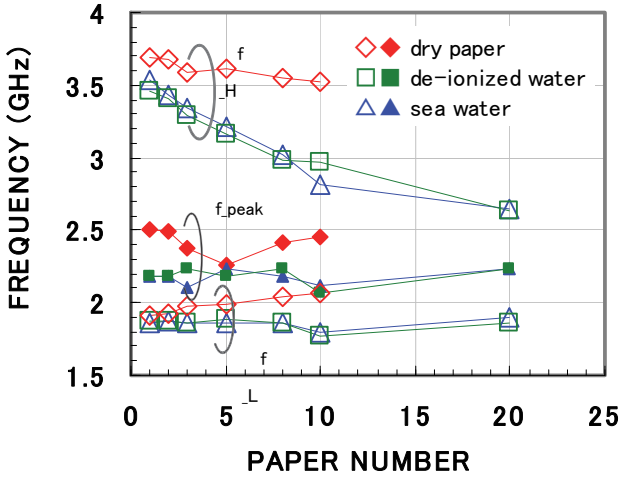

Fig.4.8. The peak frequency (f-peak) and the frequency of -3dB from the peak value.

The thickness of a paper sheet was measured as 0.02mm. The actual board spacing, however, was not measured in these experiments, so we will specify spacing only by the inserted sheet numbers.

For a reference, we measured the transmission between two SMA connectors connected by a 50 Ω micro-strip line with the same distance as the set of ECOR boards. The loss measured on the reference board was 0.62 dB at 2.45GHz as shown in Figs. 4.3 to 6. Without any paper, ECOR insertion loss was 1.05dB, which is also shown in Figs. 4.3 to 4.6. The bandwidth, defined as the difference of the frequencies where S21 is 3dB lower than the peak value, was found to be 1.80GHz, from 1.88GHz to 3.68GHz. The bandwidth is defined as this value throughout this paper. For our ECOR design, the transmission band is designed as a Butterworth-type, so there is no clear peak. The peak frequency may not be meaningful in this measurement.

With 10 sheets of dry paper, the loss increases to only 1.29 dB and the bandwidth shrinks to 1.45GHz as shown

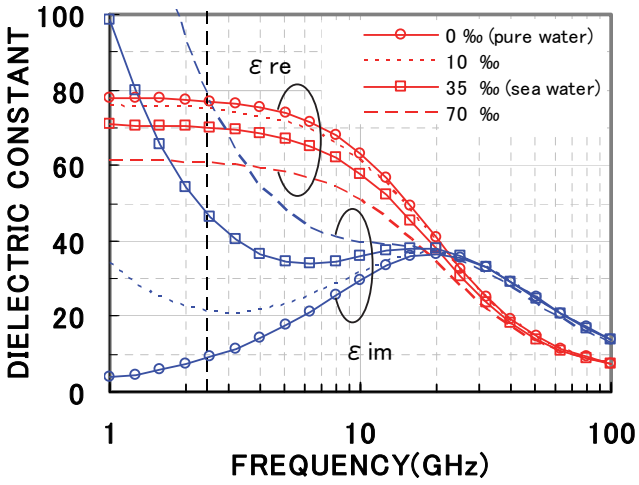

Fig.4.9. Dielectric constants of water as functions of frequency for salinities of 0 ‰(pure water), 10 ‰, 35 ‰(sea water), and 70 ‰.

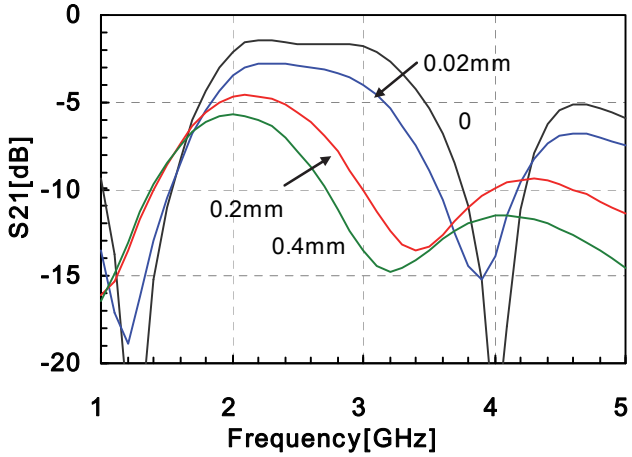

Fig.4.10. Simulated transmission through seawater. The values indicate the water layer thickness between the PE plates. The water is assumed to have 30 S/m conductivity.

in Fig.4.3. The band shrinks almost symmetrically, 0.19GHz for the lower frequency side (f_L) and 0.16GHz for the higher frequency side (f_H).

When the sheets of papers were immersed in de-ionized water, the peak S21 value decreased and the bandwidth shrank as shown in Fig. 4.4. The peak S21 decreased to 2.87dB for 10 sheets and 3.00dB for 20 sheets. Also, the band shrank to 1.20GHz for 10 sheets and 0.78GHz for 20 sheets. In this case, the shrinking occurred almost entirely on the higher frequency side; this is due to two factors: 1) the transmission band shrinks due to the reduction of the coupling coefficient by the increase in board spacing, and 2) an increase in the effective dielectric constant by the water layer.

For the measurements using tap water, the variations were almost the same as the results for de-ionized water as shown in Fig. 4.5. For the sea water case, S21 reductions were even greater as shown in Fig. 4.6. However, the transmission band defined before is almost the same as that observed with de-ionized water. The variations of peak S21 and the transmission frequencies are shown in Figs. 4.7 and 4.8, respectively. The results for tap water are almost the same as those of de-ionized water.

4.4 Electromagnetic simulation

Electromagnetic simulations were carried out to compare with the experimental results. The complex dielectric constant of water can be calculated from the Debye expression [15], which is given by,

$$\varepsilon = \varepsilon_\infty + \frac{\varepsilon_S - \varepsilon_\infty}{1 + j\omega\tau} - j\frac{\sigma}{\omega\varepsilon_0} \qquad (1)$$

where $\omega = 2\pi f$ is the angular frequency, ε_∞ is the dielectric constant at infinite frequency, ε_S is the static dielectric constant, τ is the relaxation time, σ is the ionic conductivity, and ε_0 is the permittivity of free space. The values of ε_S, τ and σ are all functions of the temperature and salinity of water. The dielectric constants, both real

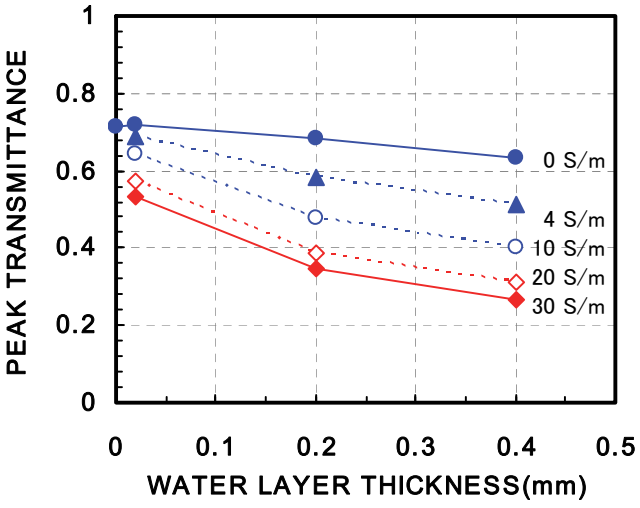

Fig.4.11. Simulated peak transmittance through waters with various conductivities.

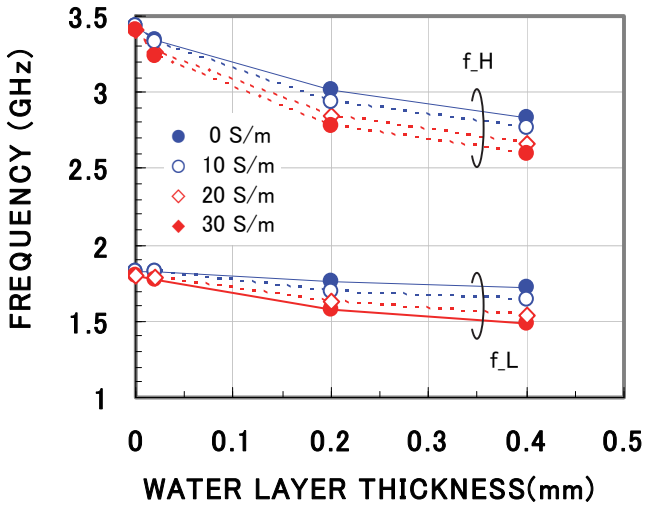

Fig.4.12. Simulated -3dB frequency through waters with various conductivities.

and imaginary parts, are shown in Fig. 4.9 for waters with various salinity values. The salinity of standard sea water is 35‰ and the conductivity σ is 5.3S/m at 25°C. For pure water, ε_{REAL}=77.1 and tanδ is 0.12 for 2.45GHz at 25°C from the parameters in Ref.3, but we used the default values of the simulator (HFSS) which are ε_{REAL}=81 and tanδ = 0.16 regardless of the frequency.

Figure 4.10 shows the simulated transmission characteristics for the case of σ=30S/m together with the tanδ = 0.16 caused by the molecular polarization. The transmission is quite similar when we translate the thickness of the water layer to 0.02 mm/sheet. The peak transmission and the 3dB frequencies are shown in Figs. 4.11 and 4.12, respectively.

4.5 Discussion

Qualitatively, similar results were obtained by experiment and simulation. As the water layer thickness increased, the transmission decreased and the band shifted to the lower frequency. The S21 degradation was larger for the water with higher conductivity, and the band width reduction value was nearly unaffected by the salinity value. However, to match the results with experiments, the assumed conductivities for both pure water and sea water were too high. There are several ambiguities in the present experiments, such as the thickness of the wet papers under clipped compression, the quality of the clean wipe paper, and the penetration of water to unintended places. Further investigation will be necessary to achieve better agreement between the experimental and modeled results.

4.6 Conclusion

The ECOR insertion loss under dry conditions was 1.05dB. If we allow for a 1dB loss increase, 5 sheets are allowed for paper soaked with de-ionized water, and 2 sheets for sea water. Under these conditions, the bandwidth shrinks mostly from the higher frequency side. So the initial bandwidth should be wider considering this shift. Wireless transmission using ECOR was originally intended to be used for non-contact transmission, but ECOR resonators may be in contact with plastic covers. The incursion of water under these circumstances should be minimized by, for instance, using moisture-resilient materials.

Although there is some disagreement between experimental and simulated results, the present experiments confirm that wet conditions may not present serious problems for the use of ECOR as a complete waterproof connector for power transmission.

Acknowledgement

We would like to thank Dr. Ikuo Awai of Ryutech Corp., Prof. Naoki Shinohara, Dr. Hiroshi Tonomura and Dr. Teruo Fujiwara for their valuable discussion. We would also like to thank Dr. Gregg Jessen of AFRL for his encouragement on this work.

References

[1] Y. Iwasaki, M. Abe, K. Hayashino, K. Fukui, J. Ao and Y. Ohno, "60 GHz Wireless Interconnection Using Electromagnetic Coupling of Open-Ring Resonators," SSDM2012(Sept.25, Kyoto, Japan) PS-5-10 (2012)

[2] Y. Okuyama, J-P. Ao, I. Awai and Y. Ohno, "Wireless Inter-Chip Signal Transmission by Electromagnetic Coupling of Open-Ring Resonators," *Japanese Journal of Applied Physics*, vol.48, 04C025,

[3] A. Karalis, J. D. Joanopoulos and M.Soljacic, "Efficient wireless non-radiative mid-range energy transfer," *Annals of Physics*, vol.323, pp.34-48, (2008)

[4] Y. Ohno, I. Awai, "Wireless Interconnection by Electromagnetic Coupling of Open-Ring Resonators and Its Application to System," 2009 International Conference on Solid State Devices and Materials, (SSDM 2009), D-2-1, Sendai, Japan (2009)

[5] I. Awai and A. K. Saha, Proceedings of Asia-Pacific Microwave Conference (APMC 2006), p.167 – 172 (2006)

[6] M. Abe, T. Amou, K. Kuramoto, J.-P. Ao and Y. Ohno, " Effects of Substrate Conductivity on Open-Ring Resonator Wireless Interconnection," 2010 Asia-Pacific Radio Science Conference, (AP-RASC'10), D1-6, Toyama, Japan (2010)

[7] M. Abe, Y. Okuyama, J-P. Ao and Y. Ohno, "Misalignment effects in inter-chip wireless connection with open-ring resonators," 2010 Asia-Pacific Microwave Conference Proceedings, (APMC 2010), 908 - 911, Yokohama, Japan (2010)

[8] K. Fukui, Taro Takeuchi, K. Hayashino, K.Harauchi, Y. Iwasaki, J-P Ao, and Y. Ohno, "T-shaped Anode GaN Schottky Barrier Diode for Microwave Power Rectification," IMWS-IWPT 2012, FRI-F-23, Kyoto, Japan (2012)

[9] K. Harauchi, et. al., "Power Transmission through Insulating Plate Using Open-Ring Resonator Coupling and GaN Schottky Diode, " IMWS-IWPT 2011, May 12-13, 2011 – Uji (Kyoto), Japan, IWPT2-2 (2011)

[10] J.-P. Ao, et. al.,"S-parameter Analysis of GaN Schottky Diodes for Microwave Power Rectification," 32nd IEEE Compound Semiconductor IC Symposium(CSICS 2010), Monterey, USA, J-4 (2010)

[11] K. Takahashi, J-P Ao, Y. Ikawa, C-Y Hu, H. Kawai, N. Shinohara, N. Niwa, and Y. Ohno, : GaN Schottky Diodes for Microwave Power Rectification, Japanese Journal of Applied Physics, Vol.48, No.4, 04C095 (2009)

[12] K. Hayashino, K.Harauchi, Y. Iwasaki, K. Fukui, J-P Ao, and Y. Ohno, "Analysis of Loss Mechanism in Rectenna Circuit with GaN Schottky Barrier Diode," IMWS-IWPT 2012, FRI-F-18, Kyoto, Japan (2012)

[13] J. O. McSpadden, L. Fan and K. Chang, "Design and Experiments of a High-Conversion-Efficiency 5.8-GHz Rectenna, IEEE Trans. on Microwave Theory and Techniques, 46, pp.2053-2060 (1998)

[14] Y. Iwasaki, T. Shioiri, K.Harauchi, K. Fukui, K. Hayashino, J-P Ao, and Y. Ohno, "Effects of Wetting to Wireless Power Transmission by Open-Ring Resonators Coupling," IMWS-IWPT 2012, FRI-E-2, Kyoto, Japan (2012)

[15] L. Klein, C. Swift, IEEE Transactions on Antennas and Propagation, Vol.25, pp.104 – 111(1977)